CD36 Identifies a Subpopulation of Adipose-Derived Mesenchymal Stromal Cells with Enhanced Osteogenic Ability.

Emily Camilleri (camilleri.emily@mayo.edu)
Mayo Clinic Rochester https://orcid.org/0000-0003-3145-0277
Scott M. Riester
Mayo Clinic Health System in Albert Lea
Michael Gustafson
Mayo Clinic Arizona
Catalina Galeano Garces
Mayo Clinic Rochester
Christopher R. Paradise
Mayo Clinic Rochester
Martina Glusevic
Mayo Clinic Rochester
Peggy Bulur
Mayo Clinic Rochester
Amel Dudakovic
Mayo Clinic Rochester
Allan B. Dietz
Mayo Clinic Rochester
Andre J van Wijnen
University of Vermont

Research Article

Keywords: Adipose-derived mesenchymal stromal cells, RNA-sequencing, subpopulation, CD36, osteogenesis

Posted Date: October 25th, 2021

DOI: https://doi.org/10.21203/rs.3.rs-987811/v1

Abstract

Background

Adipose-derived mesenchymal stromal cells (AMSCs) represent attractive cellular therapeutics for treatment of various diseases including osteoarthritis and bone degeneration. Preparation and characterization of AMSCs show donor-to-donor variability that indicating that AMSCs are heterogeneous populations of cells. Cell surface markers to identify MSCs, such as CD44, CD90, and CD105, are relatively invariable among AMSCs and do not reflect the heterogeneity of AMSC populations. CD36, a multifunctional surface receptor associated with transport of oxidized low-density lipoproteins and fatty acids, is also expressed by AMSCs but this marker is considerable more variable. Therefore, we assessed whether CD36 can be used to identify subpopulations in AMSCs.

Methods

Clinical-grade AMSCs were isolated from patient fat biopsies, cultured under xenobiotic-free conditions using human platelet lysate and sorted by flow cytometry or magnetic cell sorting to characterize CD36 expression. CD36 enriched, CD36 depleted, and unsorted AMSCs were characterized using cellular and molecular techniques including proliferation, multilineage potential, RNA-sequencing and bioinformatics, metabolomics, and sensitivity to the CD36 inhibitor sulfosuccinimidyl oleate (SSO).

Results

CD36 exhibited biphasic expression on AMSCs grown in human platelet lysate. Enrichment of $CD36^+$ AMSCs showed that $CD36^+$ expression identifies a stable subpopulation. Transcriptomic analysis revealed enhancement of calcium transporter genes. Osteogenic differentiation of $CD36^+$ enriched, $CD36^+$ depleted, and unsorted AMSCs showed strikingly enhanced osteogenic calcium deposition and enhanced expression of alkaline phosphatase (ALPL) and osteoprotegrin (TNFRSF11B) in the $CD36^+$ population. While lipid droplets were not altered, adipogenic differentiation showed upregulated gene expression of key adipogenic markers, including fatty acid-binding protein 4 (FABP4) and Adiponectin (ADIPOQ), with $CD36^+$ enrichment. Treatment of $CD36^+$ enriched AMSCs with the SSO showed reduced calcium deposition whereas $CD36^+$ depleted AMSCs were unaffected.

Conclusions

CD36 exhibits variable expression amongst AMSCs. $CD36^+$ enriched AMSCs are a stable subpopulation with enhanced osteogenic potential that linked to CD36 receptor function. These results may further refine production and clinical application of AMSC cellular therapeutics. Furthermore, the enhanced osteogenic potential of $CD36^+$ AMSCs may be considered for therapeutic regeneration of bone.

Introduction

Cell surface receptors and proteins are used as markers to define primary cells with common characteristics. The International Society of Cell Therapy (ISCT) and International Federation of Adipose Therapeutics (IFATS) describe cultured adipose-derived mesenchymal stromal cells (AMSC) by the expression of CD90/THY1, CD73/NT5E, CD105/ENG, and CD44 and absence of CD45/PTPRC and CD31/PECAM1, as well as plastic adherence and multi-lineage potential [Dominici et. al. 2006; Bourin et. al. 2013; Baer et. al. 2014]. Expression of these classical surface markers are indeed hallmarks of AMSCs and previous studies on clinical-grade AMSCs utilized in clinical trials also demonstrate this immunophenotype [Camilleri et. al. 2016; Dudakovic et. al. 2014]. However, donor-to-donor variability in proliferative capacity and differentiation potential indicates that classical markers are unable to account for these differences or indicate therapeutic potential.

Previous studies characterizing the stromal vascular fraction (SVF) and AMSCs have identified other cell surface markers that exhibited variable expression and presence of subpopulations. The CD34 protein is expressed at low levels amongst endothelial cells and AMSCs [Camilleri et. al. 2016]. Isolation of CD34+ cells from the SVF, AMSC, and bone marrow derived mesenchymal stromal cells (BMSCs), were able to undergo tri-lineage differentiation [Busser et. al. 2015]. CD146, a pericyte marker, was also found to be variably expressed indicating two subpopulations within the SVF [Astori et. al. 2007]. Positive selection of $CD90^+$ AMSCs were found to have enhanced osteogenic potential compared to unsorted, $CD105^+$ or $CD105^-$ cells [Chung et. al. 2013]. In addition, SSEA-4^+ was also found to identify an osteogenic subpopulation [Mihaila et. al. 2014; Mihaila et. al. 2013]. Rada and colleagues [2011] utilized immunomagnetic sorting to isolate 8 different subpopulations based upon the expression of CD29, CD44, CD49d/ITGA4, CD73, CD90, CD105, STRO-1/HSPA8 or p75. Each subpopulation isolated exhibited differences in differentiation potential, where STRO-1^+ cells were found to have enhanced osteogenic matrix production [Rada et. al. 2011]. Similarly, Canepa and colleagues [2021] utilized cytometry time-of-flight to identify an osteogenic population of AMSCs characterized by the expression of just two markers: ALP^+(ALPL)/$CD73^+$. Together, studies support the presence of functional subpopulations within classically defined AMSCs.

CD36 is a surface receptor that recognizes and binds multiple ligands and thus exhibits multiple functions depending on the cell type and context. The most notable function of CD36 is as a fatty acid transporter where CD36 recognizes and bind to long chain fatty acids that are internalized and either metabolized or stored [Pepino et. al. 2014]. Other ligands recognized by CD36 include thrombospondin, collagen, fibronectin, and pathogen-associated lipids [Pepino et. al. 2014]. Furthermore, CD36 is uniquely expressed on AMSCs and may be used to distinguish them from BMSCs and other cell types [Bourin et. al. 2013; Camilleri et. al. 2016]. Recently, $CD36^+$ was identified as a marker human adipocyte progenitors following an unbiased screen single cell screen on passaged AMSCs [Gao et. al. 2017]. The variable expression of CD36 in clinical grade AMSCs suggests functional specialization among AMSCs that has not yet been explored.

In this study, we hypothesized that $CD36^+$ identifies a stable AMSC subpopulation that may affect its potential to differentiate into adipogenic or osteogenic linages. Our results show that while $CD36^+$ AMSCs retains both osteogenic and adipogenic differentiation potential, these cells exhibit enhanced matrix mineralization that is mediated by CD36 receptor function.

Methods

Primary MSC culture conditions

The Mayo Clinic Institutional Review Board (IRB) approved protocols for the collection of fat biopsy or bone marrow from consenting donors and clinical trial participants utilized in this study. Adipose- or bone marrow-derived mesenchymal stromal cells were isolated as previously described [Camilleri et. al. 2016; Dudakovic et. al. 2014; Crespo-Diaz et. al. 2011]. Cells were expanded using standard operating procedures used for the culture of MSCs for clinical use. Primary AMSC or BMSCs were maintained in standard culture media composed of Advanced MEM (Gibco) with 5% human platelet lysate (Mill Creek Life Sciences), 2 mM L-glutamine (Invitrogen), 2U/mL heparin (NovaPlus®) and antibiotics (100 U/ml penicillin, 100 g/ml streptomycin) and maintained at 37°C in 5 % CO_2. Table 1 describes the patient information of AMSCs utilized in these studies.

Flow cytometry for MSC characterization

AMSCs and BMSCs were harvested from culture for flow cytometry characterization as previously described [Camilleri et. al. 2016]. Briefly, ~1 × 10^6 cells were pelleted and the supernatant was removed, before incubation with 50µL of mouse serum for 5 min at room temperature. Primary antibody mixes were prepared as described in Supplemental Table 1 and were added to respective tubes, mixed, and incubated for 15 min at room temperature in the dark. Stained cells were washed with a total of 3 ml of PBSFE [PBS with 5 mM NaEDTA (Sigma) and 1% bovine serum albumin (Sigma)], centrifuged, and supernatant was discarded. Cells were resuspended in 200µL of 1% paraformaldehyde (Electron Microscopy Sciences) prior to acquisition. The Beckman Coulter Gallios (Beckman Coulter) flow cytometer was used to acquire 50,000 AMSC events and the Kaluza software (Beckman Coulter) was used to define population gates (% Gated) and mean fluorescence intensity (MFI) values.

Magnetic and Fluorescence Cell Sorting

$CD36^+$ AMSCs were enriched using either magnetic or fluorescence-sorting techniques and specified in the results section. For both isolation techniques, the CD36-APC antibody (A87786, Beckman Coulter) was utilized. Magnetic cell sorting was performed on three AMSC donors (540, 258, 211) at passage four or five. Prior to sorting, cells were maintained in standard culture medium and expanded in T-175 flasks. Cells were collected by TrypLE (Gibco), centrifuged, and washed once with ice cold Advanced MEM with no supplements. After centrifugation, cells were resuspended in ice cold Advanced MEM and filtered using a 40µm cell strainer. Cells were counted and 1x10^7 cells were transferred to a new tube and loosely pelleted, while the supernatant was discarded. Cells were gently agitated, 50µL of CD36-APC antibody was added, quickly vortexed to mix, and incubated for 15 minutes in the refrigerator in the dark. Following incubation, cells were washed twice with ice cold Advanced MEM. Cell pellets were gently agitated and 20µL of anti-APC microbeads (MACS Miltenyi Biotec) were added per 1x10^7 cells. After brief vortexing, cells were incubated for 15 minutes at 4°C in the dark. Cells were then washed as described above and up to 1x10^8 cells were resuspended in 500µL of Advanced MEM. CD36 positive cells were selected using the autoMACS Separator (MACS Miltenyi Biotec) and the negative fraction was also collected. Immediately following magnetic sorting, fractions of cells were analyzed by flow cytometry to evaluate CD36 levels. Cells were incubated with CD90-FITC (BD Pharmingen), CD140b-PE (PDGFRB; BD Biosciences), CD44-PerCP Cy5.5 (BD Pharmingen), and CD36-APC (Beckman Coulter) in the dark for 15 minutes. Following incubation, cells were washed with PBS and centrifuged, while the supernatant was discarded. Antibody labelled cells were resuspended in PBS for analysis on the FACS Calibur (BD Biosciences)

flow cytometer. Supplemental table 2 shows the enrichment of $CD44^+/CD36^+$ cells for the magnetic separated AMSC populations.

Fluorescence sorting of one AMSC donor (540) was performed. AMSCs at passage five were expanded in vitro in T-175 flasks until 90% confluent. Cells were harvested, filtered with a 40µm cell strainer, counted, then pelleted and resuspended in PBS, and $4x10^6$ cells were transferred to a new tube. Cells were then pelleted and resuspended in 400µL of PBS and stained with CD36-APC (Beckman Coulter) as previously described. Following incubation, cells were washed with PBS and resuspended in 500µL for cell sorting. The BD FACSAria (BD Biosciences) sorter was used to isolate AMSCs based on CD36 staining intensity: negative, dim, and bright. Cells were sorted into growth medium and then expanded as previously described. Supplemental table 2 shows the enrichment of the populations.

Incucyte

AMSCs were seeded onto 6-well plates at 3,000 cells/cm^2 in filtered (0.2µm) medium and placed in the Incucyte (Satorius) system maintained at 37°C in 5% CO_2. The Incucyte was programmed using the Confluence (v1.5) package to image cells every three hours to assess cell culture confluence. Doubling time was calculated by fitting a line to the slope when cells were between 40-80% confluent with R^2 greater than 0.98.

Immunofluorescence

Expression of cell surface markers, CD44 or CD36, on AMSCs were visualized using immunofluorescence staining. Briefly, AMSCs were seeded onto glass coverslips and allowed to adhere until ~90% confluent. Cells were fixed with 4% paraformaldehyde, washed in PBS with 0.2% v/v Tween-20, and blocked with 10% normal goat serum (NGS) in PBS with 0.2% v/v Tween-20 for one hour. Primary antibodies CD44 (BD Pharmingen, 559046) or CD36 (Abcam, ab23680) were diluted in wash buffer (1% NGS in PBS with 0.2% v/v Tween-20) added to coverslips and incubated overnight at 4°C. Coverslips were rinsed with wash buffer and secondary antibodies diluted in wash buffer were added to coverslips, including goat anti-mouse AlexaFluor 488 (ThermoFisher) or donkey anti-mouse AlexaFluor® 555 (ThermoFisher). Coverslips were incubated for one hour at room temperature in the dark, washed with PBS, and mounted with ProLong Gold with DAPI (Invitrogen) onto a microscope slide. Fluorescence images were obtained using an inverted Zeiss LSM 780 laser-scanning confocal microscope (Carl Zeiss).

Osteogenic differentiation

AMSCs were seeded on 6- or 12-well plates at 3,000 cells/cm^2 in standard culture medium until plate was confluent. Upon confluence (day 0), medium was replaced with osteogenic induction medium [standard culture medium supplemented with 50µg/mL ascorbic acid, 4mM beta glycerophosphate, and 10nM dexamethasone] and fresh osteogenic medium was changed every three days. Calcium deposition was detected using Alizarin Red staining at day fourteen as previously described [Dudakovic et al 2015].

Adipogenic differentiation

AMSCs were seeded on 6- or 12-well plates at 3,000 cells/cm^2 in standard culture medium until plate was confluent. Upon confluence (day 0), standard medium was replaced with adipogenic medium that consisted of

standard medium supplemented with StemXVivo Adipogenic Supplement (R&D systems). Adipogenic medium was replaced every three days until further analysis. Lipid droplet formation was evaluated at day fourteen using Oil Red O staining as previously described [Dudakovic et al 2015].

Sulfosuccinimidyl oleate sodium (SSO) inhibitor studies

The CD36 inhibitor SSO (Santa Cruz Biotechnology) was reconstituted with DMSO, and DMSO was used as a negative control for these experiments. To optimize the SSO concentration, AMSCs were seeded onto 96-well plates and upon confluence were treated concentrations ranging from 12.5μM to 200μM SSO or DMSO. Viability/metabolic activity was evaluated after 24 hours using CellTite96®AQueous non-radioactive cell proliferation (MTS) assay (Promega). For osteogenic differentiation with DMSO or 200μM SSO, AMSCs were plated onto 12-well plates in standard medium at 3,000 cells/cm^2. The following day, medium was replaced with standard medium containing either DMSO or 200μM SSO. After three days (day 0), medium was replaced with osteogenic medium as described above and new osteogenic medium replaced every three days. Alizarin Red staining was performed at day fourteen.

Mass Spectroscopic Analysis of Acylcarnitines and Tricarboxylic Acid (TCA) metabolites

$CD36^+$ enriched, $CD36^+$ depleted, or unsorted AMSCs were established as described above for donor 211 expanded in T-175 flasks. For mass spectroscopic analysis, AMSCs and subpopulations were trypsinized and five cell pellets each containing $5x10^6$ cells were snap frozen in LN2 and stored at -80°C before analysis.

Acylcarnitines analysis was performed as previous described [Chace et. al. 2001]. Briefly, cell pellets were lysed in 1xPBS then internal standard solution was added. Proteins were removed by adding a solution of methanol/acetonitrile (v/v) to the sample mixture. The sample was centrifuged at 12,000 rpm for 10 mins at 4 °C, supernatant transferred to a 1 dram vial, and dried with N_2. Samples were reconstituted and analyzed on a Waters Acquity UPLC system coupled with a Thermo Quantiva tandem mass spectrometer in positive (H)ESI mode. Concentrations of carnitine (162.11 to 85.02 *m/z*), acetylcarnitine (204.12 to 85.02 *m/z*), propionylcarnitine (218.14 to 85.02 *m/z*), butyrylcarnitine (232.15 to 85.02 *m/z*), isovalerylcarnitine (246.17 to 85.02 *m/z*), octanoylcarnitine (288.22 to 85.02 *m/z*), lauroylcarnitine (344.28 to 85.02 *m/z*), myristoylcarnitine 372.36 to 85.02 *m/z*), palmitoylcarnitine (400.39 to 85.02 *m/z*), oleoylcarnitine (426.39 to 85.02 *m/z*), and stearoylcarnitine (438.39 to 85.02 *m/z*) were measured against a 11-point calibration curve that underwent the same preparation.

Analysis of TCA was performed as described previously [Koek et. al. 2006]. Briefly, cell pellets were washed with 1x PBS twice prior to being lyzed in 1x PBS after spiking in an internal solution containing U-13C labeled analytes. The proteins were removed by adding 250 μL of chilled methanol and acetonitrile solution to the sample mixture. After drying the supernatant in the speed vac, the sample was derivatized with ethoxime and then with MtBSTFA + 1% tBDMCS (N-Methyl-N-(t-Butyldimethylsilyl)-Trifluoroacetamide + 1% t-Butyldimethylchlorosilane) before it was analyzed on an Agilent 5975C GC/MS (gas chromatography/mass spectrometry) under electron impact and single ion monitoring conditions. Concentrations of lactic acid (m/z 261.2), fummaric acid (m/z 287.1), succinic acid (m/z 289.1), oxaloacetic acid (m/z 346.2), ketoglutaric acid (m/z 360.2), malic acid (m/z 419.3), cis aconitic acid (m/z459.3), citric acid (m/z 591.4), and isocitric acid (m/z

591.4), glutamic acid (m/z 432.4) were measured against a 7-point calibration curves that underwent the same derivatization.

Transmission Electron Microscopy

$CD36^+$ enriched, $CD36^+$ depleted, and unsorted AMSCs were seeded onto 6-well plates at approximately 3,000cells/cm^2 and allowed to proliferate for three days. AMSC subcellular structures were assessed using digital electron microscopy (Phillips CM10) at the Mayo Clinic Electron Microscopy Core. Briefly, cells were fixed in Trump's fixative and mounted on mesh grids. Six-eight representative fields of view from each of the populations were randomly selected and visually examined.

Real-time reverse transcriptase quantitative PCR analysis

Total RNA was isolated from AMSCs using Trizol® Reagent (Thermo) and purified using the Direct-zol mini kit (Zymo). The SuperScript III First-Strand Synthesis System (Invitrogen) was used to reverse transcribe RNA into cDNA and used as template for real-time PCR analysis. Real-time reactions were performed with 10 ng cDNA per 10 µl with the QuantiTect SYBR Green PCR Kit (Qiagen) and gene specific primers [Supplemental Table 3]. Reactions were detected using the CFX384 Real-Time System (BioRad). Gene expression levels were normalized to the housekeeping gene, AKT1, and quantified using the 2^(−delta delta Ct) method.

High throughput RNA sequencing

Total RNA from AMSC subpopulations were subjected to RNA-sequencing using the TruSeq RNA Sample Prep Kit v2 (Illumina) and were analyzed using Illumina HiSeq 2000 with TruSeq SBS Kit v3 and HCS v2.0.12 data collection software. Sequence data were processed using MAPRSeq (v.1.2.1) and a bioinformatics workflow (TopHat 2.0.6, HTSeq, and edgeR 2.6.2), where expression data were normalized using the fragments per kilobase per million (FPKM) method. Differential gene expression analysis was performed using gene count data and analyzed with DESeq2 (v1.26.0) package in RStudio (v1.2.5033) with a p-value set at 0.05.

Statistical analysis

Statistical analyses were performed using Prism 9.2 (GraphPad) software and nonparametric, Mann-Whitney test was used to determine differences in qPCR and metabolomics data. Linear regression was used to analyze Incucyte population doubling data at the exponential phase of cell growth.

Results

$CD36^+$ classifies a stable subpopulation of clinical grade AMSCs grown in human platelet lysate

Clinical-grade AMSCs have previously been shown by our laboratory to express classical MSC surface markers [Camilleri et. al. 2016; Dudakovic et. al. 2014] including CD44 (Figure 1A) and were also previously demonstrated to exhibit tri-lineage (i.e., adipogenic, chondrogenic, and osteogenic) potential [Dudakovic et. al. 2015]. Flow cytometric analysis of CD44 and CD36 revealed biphasic expression of CD36 and a distinct $CD36^{bright}$ cell population (Figure 1B) that is highly variable between donors. RNA-sequencing of MSCs derived from donors represented in Figure 1B also demonstrates increased abundance of CD36 transcript in 540 compared to 536,

whereas expression of CD44 and CD90 were more similar between donors (Figure 1C). We observed BMSCs grown in hPL did not express CD36 (Figure 1D).

$CD36^+$ AMSCs were enriched by magnetic separation and growth potential of these cells was compared to unsorted and $CD36^+$ depleted cells (this fraction may also contain cells with low abundance of CD36) (Figure 2A and Supplemental table 2). Serial passaging and flow cytometry analysis revealed that $CD36^+$ enriched AMSCs maintained enrichment of $CD90^+/CD36^+$ cells compared to unsorted and $CD36^+$ depleted AMSCs. In comparison, expression of $CD90^+/CD140b^+$ (PDGFRB) were similar between the AMSC fractions over the four passages (Figure 2B), with the exception of passage eight. $CD140b^+$ was evaluated for comparison as a non-classical marker for AMSCs that was previously shown to exhibit variable expression on AMSCs [Camilleri et. al. 2016]. Furthermore, we observed no difference in doubling time between unsorted, $CD36^+$ depleted and $CD36^+$ enriched cells (Supplemental figure 1). Together, these data strongly supports the identification of a stable $CD36^+$ enriched AMSC subpopulation.

Since CD36 binds and transports fatty acids, we performed transmission electron microscopy (TEM) and metabolomic analysis to identify changes in intracellular metabolism. Evaluation of AMSCs by TEM did not reveal obvious changes in lipid storage or abundance of mitochondria in $CD36^+$ enriched AMSCs compared to $CD36^+$ depleted or unsorted cells (Supplemental figure 2). Metabolomic analysis of acetylcarnitines, ranging from stearoylcarnitine (C18) to carnitine (C0), were not significantly different between $CD36^+$ enriched and depleted subpopulations except for Butyrylcarnitine (C4) (Supplemental table 4). Analysis of TCA metabolites showed increased in citrate abundance in $CD36^+$ enriched AMSCs, although downstream metabolites were only slightly elevated (Supplemental table 4). In sum, these results suggest that $CD36^+$ enriched AMSCs do not exhibit major metabolic changes in fatty acid storage, oxidation of long chain fatty acids or energy production.

$CD36^+$ enriched AMSCs show higher expression of calcium transport genes

Transcriptomic analysis was performed to evaluate differences in gene expression between $CD36^+$ enriched and depleted AMSCs, and unsorted AMSCs were also included for comparison. Proliferating and confluent samples of these cell types were analyzed to account for gene expression that may occur upon confluence. $CD36^+$ enriched AMSCs were found to exhibit greater than 2-fold expression 45 genes compared to $CD36^+$ depleted AMSCs. Conversely, 110 genes were expressed greater than 2-fold in $CD36^+$ depleted AMSCs compared to enriched AMSCs. $CD36^+$ enriched AMSCs showed enhanced expression of calcium transport or channel genes including TRPC6, SLC24A3 (NCKX3), CACNA1H, endothelial proteins such as GPR116 (ADGRF5) and ACTG2, and transcription factors including MEOX2 and MYOCD (Figure 2C and data not shown). Whereas expression of genes including PLA2G2A, PLA2G5, PTGFR, GPR133(ADGRD1), and STEAP4 (Figure 2C and data not shown) was higher in $CD36^+$ depleted AMSCs. Immune regulatory genes including IL1RL1, CXCL14, CXCL12, IL33, CXCR7 were also enhanced in $CD36^+$ depleted AMSCs (data not shown). Functional annotation clustering of differentially expressed genes greater than 1.5-fold in either $CD36^+$ enriched or depleted AMSCs was also performed. $CD36^+$ enriched AMSCs showed modest enrichment of functional categories involved in cell membrane proteins and calcium transport (Table 2). Conversely, $CD36^+$ depleted AMSCs are involved in extracellular matrix interactions including proteases and fibronectin, as well as lipid metabolism (including

APOE, PLA2G2A, PLA2G5, HSD11B1). Together, our studies suggest that CD36^{+} enriched AMSCs have enhanced expression of calcium transport and endothelial proteins and transcription factors.

CD36^{+} enriched AMSCs exhibit enhanced osteogenic potential

We evaluated the osteogenic and adipogenic differentiation potential of CD36^{+} enriched, CD36^{+} depleted and unsorted AMSCs. Osteogenically differentiated CD36^{+} enriched cells exhibited enhanced mineral deposition as shown by alizarin red staining when compared to depleted or unsorted AMSCs (Figure 3A). Gene expression analysis revealed elevated abundance of CD36 transcript over a 21-day time course in CD36 enriched AMSCs compared to other AMSC populations (Figure 3B). Furthermore, expression of alkaline phosphatase (ALPL) was upregulated in CD36 enriched cells at day zero, suggesting an enhanced in osteogenic potential compared to other fractions. Osteoprotegrin (OPG) was also enhanced in CD36^{+} enriched cells. Together, these data indicate that CD36^{+} enriched AMSCs have enhanced osteogenic potential.

Adipogenic differentiation of CD36^{+} enriched AMSCs did not show differences in fat droplet formation at day 14 of differentiation (Figure 3C). However, expression of characteristic adipogenic transcription factors and proteins including peroxisome proliferator-activated receptor gamma (PPARG), fatty acid binding protein 4 (FABP4), and adiponectin (ADIPOQ) were enhanced compared to unsorted and CD36^{+} depleted AMSCs (Figure 3D). This finding suggests that CD36^{+} enriched subpopulation may have elevated expression of adipogenic genes.

Enhanced osteogenic potential may be mediated by CD36 activity

To investigate the role of CD36 receptor in promoting osteogenesis of AMSCs, we compared CD36 fractions following treatment with the CD36 inhibitor, SSO. Flow cytometry cell sorting was used to isolate AMSC subpopulations with no (negative), dim or bright CD36 expression (Supplemental table 2). Treatment with various concentrations of SSO for 24 hours did not alter metabolic activity of the negative or dim populations. However, CD36^{bright} AMSCs showed higher metabolic activity compared to the other populations and SSO (200μM) reduced the metabolic activity to a similar level as CD36 negative and dim AMSCs (Figure 4A). These data suggest that CD36 activity may mediate differences in metabolic activity of AMSCs.

We also evaluated the role of CD36 in modulating osteogenic potential of AMSCs in the presence of the SSO inhibitor. CD36^{bright} or negative subpopulations were osteogenically induced in the presence of SSO for the first three days of differentiation (day -3 to day 0), after which they continued differentiating in osteogenic medium for up to 21 days. Matrix mineralization was considerably reduced in CD36^{bright} AMSCs treated with SSO compared to CD36^{negative} AMSCs which appear unchanged (Figure 4B). Inhibition of CD36 activity with SSO induced the expression of CD36 in both subpopulations at confluence (day 0), where CD36^{bright} cells were more sensitive SSO treatment. At day 21 of culture expression of osteogenic extracellular matrix genes ALPL and OPG were reduced in CD36^{bright} and not CD36^{negative} cells. RUNX2 transcript abundance was also reduced in both populations treated with SSO, especially on days 7 and 21 of culture (Figure 4C). Together, CD36 receptor activity may modulate matrix mineralization and expression of osteogenic genes.

Discussion

Adipose-derived cellular therapeutics used for clinical applications include fat grafts, purified SVF, or MSCs. Whilst the therapeutic efficacy between these products are unclear, we have shown in that cultured AMSCs exhibit phenotypic differences between donors with variable expression of other surface markers including CD36 and CD271 [Camilleri et. al. 2016; Watson et. al. 2013]. The variability in these characteristics indicate that AMSCs are a heterogenous population of cells. The identification and characterization of AMSC subpopulation has translational significance for the quality assurance of AMSC production and clinical application of AMSC therapies [Baer et. al. 2013; Walmsley et al 2015]. Surface markers that identify subpopulations with enhanced cellular characteristics such as proliferation and differentiation may be used as quality control measures for AMSC production and therapeutic efficacy. Furthermore, enrichment of subpopulations with functional differences including immunomodulatory effects or enhanced lineage differentiation, would allow the customization of AMSC cellular therapies for disease specific applications.

CD36 expression was initially described as a cell surface marker to distinguish AMSCs from BMSCs [Pachon-Pena et. al. 2011] and was also found to have variable expression on AMSCs [Bourin et. al.; Baer et. al. 2013]. However, the specific role of $CD36^+$ AMSCs has only recently been evaluated [2016]. Gao and colleagues [2016] performed an unbiased single cell cloning screen of AMSCs at passage 11 that lead to the identification of a $CD36^+$ population characterized by pronounced adipogenic differentiation and triglyceride accumulation. However, Gao and colleagues [2016] did not report on the differentiation potential of these cells for other lineages. The AMSCs evaluated in Gao and colleagues [2016] may be predisposed to adipogenesis and lipid storage due to the late passage, high population doublings, or the biologically important difference that their cells were grown in FBS. Interestingly, they demonstrated that CD36 expression on AMSCs varied depending on the anatomical location of the fat tissue, where femoral fat derived AMSCs exhibited the highest levels of CD36 expression [Gao et al. 2017]. Here, we identified the biphasic expression of CD36 amongst 15 clinical-grade AMSCs grown in hPL. Enrichment and continuous passage of $CD36^+$ AMSCs demonstrated the subpopulation maintained CD36 positivity, indicating the stability of a $CD36^+$ subpopulation. We also observed enhanced expression of adipogenic genes including PPARG, ADIPOQ, and FABP4 in $CD36^+$ enriched AMSCs, although lipid droplet formation was not enhanced. Furthermore, metabolomics analysis did not indicate that fatty acid metabolism was enhanced in $CD36^+$ enriched AMSCs compared to unsorted or $CD36^+$ depleted AMSCs.

Osteogenic differentiation of $CD36^+$ enriched AMSCs has not previously be characterized. Initial characterization of CD36 germline knockout mice identified elevated levels of cholesterol, triacylglycerol, fatty acids compared to wild-type mice [Febbraio et. al. 1999]. However, other studies of these same mice did not observe differences in total cholesterol or cholesterol related lipoproteins [Kevorkova et. al. 2013]. CD36 knockout mice were also found to have a low bone mass phenotype with reduced osteoblasts on trabecular surface and the expression of bone markers and mineralization staining were also reduced in CD36 deficient BMSCs [Kevorkova et. al. 2013]. As CD36 is not typically expressed on the cell surface of BMSCs, the specific function of CD36 in these cells and the mechanisms through which CD36 affects skeletal development is unclear. Hormone signaling from adipose tissue or other $CD36^+$ cells including vascular endothelial cells, may play a role bone development in CD36 deficient mice [Kevorkova et. al. 2013]. Recently, oxidized low density lipoproteins were found to inhibit MSC differentiation through CD36 mediated suppression of LRP5/6 and Frizzled [Dawodu et. al. 2019]. Further studies are required to evaluate the role of CD36 on AMSCs compared to MSC derived from other anatomical locations.

As a receptor, CD36 recognizes multiple ligands including fatty acids, oxidized lipoproteins, and extracellular matrix proteins [Lawler and Lawler 2012]. Activation of CD36 was previously shown to regulate membrane calcium influx which promotes phospholipase A2 to release arachidonic acid thereby promoting prostaglandin E2 production [Kuda et. al. 2011]. Furthermore, CD36 signaling may lead to the activation of mitogen activated protein kinase (MAPK) and AMP-activated protein kinase (AMPK) pathways, thereby modulating lipid and/or calcium storage [Kuda et. al. 2011; Samovski et. al. 2015]. Since modest changes in osteogenic gene expression were observed, enhanced osteogenic matrix mineralization by $CD36^+$ enriched AMSCs may be due to post-transcriptional changes to extracellular matrix proteins or signaling cascades that activate in calcium storage or export. Transcriptomic analysis of $CD36^+$ enriched and depleted AMSCs showed upregulation of genes encoding the calcium channel/exchangers or transport including TRPC6, SLC24A3 (NCKX3), and CACNA1H. Recently, CD36 was found to modulate palmitate induced activation of TRPC6 and elevation of intracellular calcium [Su et. al. 2020]. Genetic knockout of NCKX3 in mice was not found to largely modulate skeletal development due to compensation by other calcium transporting genes [Yang et. al. 2017]. However, the role of these specific calcium transporting proteins and compensatory mechanisms in osteogenesis and bone formation is largely underexplored. Nonetheless, $CD36^+$ enriched AMSCs have the potential to be utilized in orthopedic pre-clinical and clinical studies such as bone repair, where calcium deposition could promote bone regeneration.

$CD36^+$ depleted AMSCs were found to exhibit higher expression of genes involved in prostaglandin production (PLA2G2A, PLA2G5, PTGFR) and immune regulation (IL1RL1, CXCL14, CXCL12, IL33, CXCR7). These AMSCs may be more suitable to regenerative applications such as immunomodulation or vascularization where enhanced calcium deposition is neither required nor desired. Prostaglandin signaling through prostanoid receptors are known to exert anabolic or catabolic effects on bone development and fracture healing [Feigenson et. al. 2020]. Genetic studies in mice observed that loss of prostaglandin EP1 receptor promoted bone formation, fracture healing, and protected against ovariectomy-induced osteoporosis [Feigenson et. al. 2020; Feigenson et. al. 2017; Feigenson et. al. 2019; Zhang et. al. 2015]. In addition, immunomodulatory effects of AMSC have also been evaluated in pre-clinical studies [Muller et. al. 2021]. Interestingly, $CD36^+$ depleted cells were observed to have greater transcript levels of both IL33 and IL1RL1. IL33 is known to bind to IL1RL1 and induce the expression of T-helper cells type 2 cytokines including IL-4, IL-5, and IL-13 [Schmitz et. al. 2005]. IL-33 overexpressing MSCs were also shown to promote heart function and reduce infiltration in rats with myocardial infarction [Chen et. al. 2019].

Conclusions

We identified the variable expression of CD36 amongst clinical-grade AMSCs growth in human platelet lysate and characterized a novel, stable $CD36^+$ enriched subpopulation with enhanced osteogenic potential. $CD36^+$ enriched AMSCs also undergo adipogenic differentiation and upregulate the expression of adipogenic markers but lipid droplet formation was not enhanced. We also identified differential expression of calcium transporter genes in $CD36^+$ enriched AMSCs and immunomodulatory genes in $CD36^-$ depleted AMSCs. These studies provide strong support for the presence of subpopulations within classically defined AMSC populations. $CD36^+$ enriched AMSCs could have clinical ramifications because this biologically distinct subpopulation may have different regenerative potential compared to $CD36^-$ AMSCs.

Abbreviations

AMSC – Adipose derived mesenchymal stromal cell

BMSC – Bone marrow derived mesenchymal stromal

Geo – Geometric Mean

GMP – Good manufacturing practices

hPL – Human platelet lysate

MFI – Mean fluorescence intensity

RPKM – Reads per kilobase per million mapped reads

RNA-seq – RNA sequencing

Declarations

Ethics approval and consent to participate

The Mayo Clinic Institutional Review Board (IRB) approved all and consent was obtained from fat biopsy donors and clinical trial patients.

Consent for publication

Not applicable.

Availability of Data and Materials

The RNA-sequencing data generated and analyzed during the current study are available in the Gene Expression Omnibus (GEO) repository.

Competing interests

The authors declare the following potential conflicts of interest with respect to the research, authorship, and/or publication of this article: ABD and MPG have commercial interest in Mill Creek Life Sciences, which manufactures the clinical-grade commercial platelet lysate product used for maintaining adipose tissue-derived mesenchymal stromal cells.

Funding

This work was supported by intramural funds from the Center of Regenerative Medicine at Mayo Clinic and NIH R01 grants AR049069 (AJvW), and a Mayo Clinic Centre for Regenerative Medicine fellowship (to SMR). We also appreciate the generous philanthropic support of William H. and Karen J. Eby, and the charitable foundation in their name.

Authors' contributions

ETC, SMR, AD, MPG, CGG, AGJ, CRP, MG, PB, ABD, AJvW contributed to the study design, study performance, data collection, and preparation of the manuscript. All authors read and approved the final manuscript.

Acknowledgements

All studies were performed at Mayo Clinic. We thank the members of our research groups (Xiaodong Li, Oksana Pichurin) and the Human Cellular Therapeutics laboratory (Jarrett Anderson, Greg Butler, Darcie J. Radel) at Mayo Clinic. We also thank the Mayo Clinic Metabolomics and the Genomics Research and Bioinformatics Core facilities.

References

1. Dominici M, Le Blanc K, Mueller I, Slaper-Cortenbach I, Marini F, Krause D, Deans R, Keating A, Prockop Dj, Horwitz E. Minimal criteria for defining multipotent mesenchymal stromal cells. The International Society for Cellular Therapy position statement. Cytotherapy. 2006;8(4):315-7. doi: 10.1080/14653240600855905. PMID: 16923606.
2. Bourin P, Bunnell BA, Casteilla L, Dominici M, Katz AJ, March KL, Redl H, Rubin JP, Yoshimura K, Gimble JM. Stromal cells from the adipose tissue-derived stromal vascular fraction and culture expanded adipose tissue-derived stromal/stem cells: a joint statement of the International Federation for Adipose Therapeutics and Science (IFATS) and the International Society for Cellular Therapy (ISCT). Cytotherapy. 2013 Jun;15(6):641-8. doi: 10.1016/j.jcyt.2013.02.006. Epub 2013 Apr 6. PMID: 23570660; PMCID: PMC3979435.
3. Baer PC, Kuçi S, Krause M, Kuçi Z, Zielen S, Geiger H, Bader P, Schubert R. Comprehensive phenotypic characterization of human adipose-derived stromal/stem cells and their subsets by a high throughput technology. Stem Cells Dev. 2013 Jan 15;22(2):330-9. doi: 10.1089/scd.2012.0346. Epub 2012 Oct 4. PMID: 22920587.
4. Camilleri ET, Gustafson MP, Dudakovic A, Riester SM, Garces CG, Paradise CR, Takai H, Karperien M, Cool S, Sampen HJ, Larson AN, Qu W, Smith J, Dietz AB, van Wijnen AJ. Identification and validation of multiple cell surface markers of clinical-grade adipose-derived mesenchymal stromal cells as novel release criteria for good manufacturing practice-compliant production. Stem Cell Res Ther. 2016 Aug 11;7(1):107. doi: 10.1186/s13287-016-0370-8. PMID: 27515308; PMCID: PMC4982273.
5. Dudakovic A, Camilleri E, Riester SM, Lewallen EA, Kvasha S, Chen X, Radel DJ, Anderson JM, Nair AA, Evans JM, Krych AJ, Smith J, Deyle DR, Stein JL, Stein GS, Im HJ, Cool SM, Westendorf JJ, Kakar S, Dietz AB, van Wijnen AJ. High-resolution molecular validation of self-renewal and spontaneous differentiation in clinical-grade adipose-tissue derived human mesenchymal stem cells. J Cell Biochem. 2014 Oct;115(10):1816-28. doi: 10.1002/jcb.24852. PMID: 24905804; PMCID: PMC4225070.
6. Busser H, Najar M, Raicevic G, Pieters K, Velez Pombo R, Philippart P, Meuleman N, Bron D, Lagneaux L. Isolation and Characterization of Human Mesenchymal Stromal Cell Subpopulations: Comparison of Bone Marrow and Adipose Tissue. Stem Cells Dev. 2015 Sep 15;24(18):2142-57. doi: 10.1089/scd.2015.0172. Epub 2015 Jul 28. PMID: 26086188.
7. Astori G, Vignati F, Bardelli S, Tubio M, Gola M, Albertini V, Bambi F, Scali G, Castelli D, Rasini V, Soldati G, Moccetti T. "In vitro" and multicolor phenotypic characterization of cell subpopulations identified in fresh human adipose tissue stromal vascular fraction and in the derived mesenchymal stem cells. J Transl Med. 2007 Oct 31;5:55. doi: 10.1186/1479-5876-5-55. PMID: 17974012; PMCID: PMC2198906.

8. Chung MT, Liu C, Hyun JS, Lo DD, Montoro DT, Hasegawa M, Li S, Sorkin M, Rennert R, Keeney M, Yang F, Quarto N, Longaker MT, Wan DC. CD90 (Thy-1)-positive selection enhances osteogenic capacity of human adipose-derived stromal cells. Tissue Eng Part A. 2013 Apr;19(7-8):989-97. doi: 10.1089/ten.TEA.2012.0370. Epub 2013 Jan 28. PMID: 23216074; PMCID: PMC3589870.
9. Mihaila SM, Frias AM, Pirraco RP, Rada T, Reis RL, Gomes ME, Marques AP. Human adipose tissue-derived SSEA-4 subpopulation multi-differentiation potential towards the endothelial and osteogenic lineages. Tissue Eng Part A. 2013 Jan;19(1-2):235-46. doi: 10.1089/ten.TEA.2012.0092. Epub 2012 Oct 4. PMID: 22924692; PMCID: PMC3530944.
10. Mihaila SM, Gaharwar AK, Reis RL, Khademhosseini A, Marques AP, Gomes ME. The osteogenic differentiation of SSEA-4 sub-population of human adipose derived stem cells using silicate nanoplatelets. Biomaterials. 2014 Nov;35(33):9087-99. doi: 10.1016/j.biomaterials.2014.07.052. Epub 2014 Aug 12. PMID: 25123923.
11. Rada T, Reis RL, Gomes ME. Distinct stem cells subpopulations isolated from human adipose tissue exhibit different chondrogenic and osteogenic differentiation potential. Stem Cell Rev Rep. 2011 Mar;7(1):64-76. doi: 10.1007/s12015-010-9147-0. PMID: 20396979.
12. Canepa DD, Casanova EA, Arvaniti E, Tosevski V, Märsmann S, Eggerschwiler B, Halvachizadeh S, Buschmann J, Barth AA, Plock JA, Claassen M, Pape HC, Cinelli P. Identification of ALP+/CD73+ defining markers for enhanced osteogenic potential in human adipose-derived mesenchymal stromal cells by mass cytometry. Stem Cell Res Ther. 2021 Jan 6;12(1):7. doi: 10.1186/s13287-020-02044-4. PMID: 33407847; PMCID: PMC7789251.
13. Pepino MY, Kuda O, Samovski D, Abumrad NA. Structure-function of CD36 and importance of fatty acid signal transduction in fat metabolism. Annu Rev Nutr. 2014;34:281-303. doi: 10.1146/annurev-nutr-071812-161220. Epub 2014 May 16. PMID: 24850384; PMCID: PMC4329921.
14. Gao H, Volat F, Sandhow L, Galitzky J, Nguyen T, Esteve D, Åström G, Mejhert N, Ledoux S, Thalamas C, Arner P, Guillemot JC, Qian H, Rydén M, Bouloumié A. CD36 Is a Marker of Human Adipocyte Progenitors with Pronounced Adipogenic and Triglyceride Accumulation Potential. Stem Cells. 2017 Jul;35(7):1799-1814. doi: 10.1002/stem.2635. Epub 2017 May 18. PMID: 28470788.
15. Crespo-Diaz R, Behfar A, Butler GW, Padley DJ, Sarr MG, Bartunek J, Dietz AB, Terzic A. Platelet lysate consisting of a natural repair proteome supports human mesenchymal stem cell proliferation and chromosomal stability. Cell Transplant. 2011;20(6):797-811. doi: 10.3727/096368910X543376. Epub 2010 Nov 19. PMID: 21092406.
16. Dudakovic A, Camilleri ET, Lewallen EA, McGee-Lawrence ME, Riester SM, Kakar S, Montecino M, Stein GS, Ryoo HM, Dietz AB, Westendorf JJ, van Wijnen AJ. Histone deacetylase inhibition destabilizes the multi-potent state of uncommitted adipose-derived mesenchymal stromal cells. J Cell Physiol. 2015 Jan;230(1):52-62. doi: 10.1002/jcp.24680. PMID: 24912092; PMCID: PMC4225068.
17. Chace DH, DiPerna JC, Mitchell BL, Sgroi B, Hofman LF, Naylor EW. Electrospray tandem mass spectrometry for analysis of acylcarnitines in dried postmortem blood specimens collected at autopsy from infants with unexplained cause of death. Clin Chem. 2001;47(7):1166-82. Erratum in: Clin Chem 2001 Sep;47(9):1748. PMID: 11427446.
18. Koek MM, Muilwijk B, van der Werf MJ, Hankemeier T. Microbial metabolomics with gas chromatography/mass spectrometry. Anal Chem. 2006 Feb 15;78(4):1272-81. doi: 10.1021/ac051683+.

Erratum in: Anal Chem. 2006 Jun 1;78(11):3839. PMID: 16478122.

19. Watson JT, Foo T, Wu J, Moed BR, Thorpe M, Schon L, Zhang Z. CD271 as a marker for mesenchymal stem cells in bone marrow versus umbilical cord blood. Cells Tissues Organs. 2013;197(6):496-504. doi: 10.1159/000348794. Epub 2013 May 14. PMID: 23689142.
20. Walmsley GG, Atashroo DA, Maan ZN, Hu MS, Zielins ER, Tsai JM, Duscher D, Paik K, Tevlin R, Marecic O, Wan DC, Gurtner GC, Longaker MT. High-Throughput Screening of Surface Marker Expression on Undifferentiated and Differentiated Human Adipose-Derived Stromal Cells. Tissue Eng Part A. 2015 Aug;21(15-16):2281-91. doi: 10.1089/ten.TEA.2015.0039. Epub 2015 Jun 26. PMID: 26020286; PMCID: PMC4529076.
21. Pachón-Peña G, Yu G, Tucker A, Wu X, Vendrell J, Bunnell BA, Gimble JM. Stromal stem cells from adipose tissue and bone marrow of age-matched female donors display distinct immunophenotypic profiles. J Cell Physiol. 2011 Mar;226(3):843-51. doi: 10.1002/jcp.22408. PMID: 20857424; PMCID: PMC4340690.
22. Febbraio M, Abumrad NA, Hajjar DP, Sharma K, Cheng W, Pearce SF, Silverstein RL. A null mutation in murine CD36 reveals an important role in fatty acid and lipoprotein metabolism. J Biol Chem. 1999 Jul 2;274(27):19055-62. doi: 10.1074/jbc.274.27.19055. PMID: 10383407.
23. Kevorkova O, Martineau C, Martin-Falstrault L, Sanchez-Dardon J, Brissette L, Moreau R. Low-bone-mass phenotype of deficient mice for the cluster of differentiation 36 (CD36). PLoS One. 2013 Oct 25;8(10):e77701. doi: 10.1371/journal.pone.0077701. PMID: 24204923; PMCID: PMC3808405.
24. Dawodu D, Patecki M, Dumler I, Haller H, Kiyan Y. oxLDL inhibits differentiation of mesenchymal stem cells into osteoblasts via the CD36 mediated suppression of Wnt signaling pathway. Mol Biol Rep. 2019 Jun;46(3):3487-3496. doi: 10.1007/s11033-019-04735-5. Epub 2019 Mar 7. PMID: 30847850.
25. Lawler PR, Lawler J. Molecular basis for the regulation of angiogenesis by thrombospondin-1 and -2. Cold Spring Harb Perspect Med. 2012 May;2(5):a006627. doi: 10.1101/cshperspect.a006627. PMID: 22553494; PMCID: PMC3331684.
26. Kuda O, Jenkins CM, Skinner JR, Moon SH, Su X, Gross RW, Abumrad NA. CD36 protein is involved in store-operated calcium flux, phospholipase A2 activation, and production of prostaglandin E2. J Biol Chem. 2011 May 20;286(20):17785-95. doi: 10.1074/jbc.M111.232975. Epub 2011 Mar 31. PMID: 21454644; PMCID: PMC3093854.
27. Samovski D, Sun J, Pietka T, Gross RW, Eckel RH, Su X, Stahl PD, Abumrad NA. Regulation of AMPK activation by CD36 links fatty acid uptake to β-oxidation. Diabetes. 2015 Feb;64(2):353-9. doi: 10.2337/db14-0582. Epub 2014 Aug 25. PMID: 25157091; PMCID: PMC4303974.
28. Su Y, Chen Q, Ju Y, Li W, Li W. Palmitate induces human glomerular mesangial cells fibrosis through CD36-mediated transient receptor potential canonical channel 6/nuclear factor of activated T cell 2 activation. Biochim Biophys Acta Mol Cell Biol Lipids. 2020 Dec;1865(12):158793. doi: 10.1016/j.bbalip.2020.158793. Epub 2020 Aug 13. PMID: 32800850.
29. Yang H, Ahn C, Shin EK, Lee JS, An BS, Jeung EB. NCKX3 was compensated by calcium transporting genes and bone resorption in a NCKX3 KO mouse model. Mol Cell Endocrinol. 2017 Oct 15;454:93-102. doi: 10.1016/j.mce.2017.06.006. Epub 2017 Jun 7. PMID: 28602864.
30. Feigenson M, Jonason JH, Shen J, Loiselle AE, Awad HA, O'Keefe RJ. Inhibition of the Prostaglandin EP-1 Receptor in Periosteum Progenitor Cells Enhances Osteoblast Differentiation and Fracture Repair. Ann

Biomed Eng. 2020 Mar;48(3):927-939. doi: 10.1007/s10439-019-02264-7. Epub 2019 Apr 12. PMID: 30980293; PMCID: PMC6790162.

31. Feigenson M, Eliseev RA, Jonason JH, Mills BN, O'Keefe RJ. PGE2 Receptor Subtype 1 (EP1) Regulates Mesenchymal Stromal Cell Osteogenic Differentiation by Modulating Cellular Energy Metabolism. J Cell Biochem. 2017 Dec;118(12):4383-4393. doi: 10.1002/jcb.26092. Epub 2017 May 31. PMID: 28444901; PMCID: PMC5774856.
32. Feigenson M, Jonason JH, Shen J, Loiselle AE, Awad HA, O'Keefe RJ. Inhibition of the Prostaglandin EP-1 Receptor in Periosteum Progenitor Cells Enhances Osteoblast Differentiation and Fracture Repair. Ann Biomed Eng. 2020 Mar;48(3):927-939. doi: 10.1007/s10439-019-02264-7. Epub 2019 Apr 12. PMID: 30980293; PMCID: PMC6790162.
33. Zhang M, Feigenson M, Sheu TJ, Awad HA, Schwarz EM, Jonason JH, Loiselle AE, O'Keefe RJ. Loss of the PGE2 receptor EP1 enhances bone acquisition, which protects against age and ovariectomy-induced impairments in bone strength. Bone. 2015 Mar;72:92-100. doi: 10.1016/j.bone.2014.11.018. Epub 2014 Nov 29. PMID: 25446888; PMCID: PMC4437532.
34. Müller L, Tunger A, Wobus M, von Bonin M, Towers R, Bornhäuser M, Dazzi F, Wehner R, Schmitz M. Immunomodulatory Properties of Mesenchymal Stromal Cells: An Update. Front Cell Dev Biol. 2021 Feb 9;9:637725. doi: 10.3389/fcell.2021.637725. PMID: 33634139; PMCID: PMC7900158.
35. Schmitz J, Owyang A, Oldham E, Song Y, Murphy E, McClanahan TK, Zurawski G, Moshrefi M, Qin J, Li X, Gorman DM, Bazan JF, Kastelein RA. IL-33, an interleukin-1-like cytokine that signals via the IL-1 receptor-related protein ST2 and induces T helper type 2-associated cytokines. Immunity. 2005 Nov;23(5):479-90. doi: 10.1016/j.immuni.2005.09.015. PMID: 16286016.
36. Chen Y, Zuo J, Chen W, Yang Z, Zhang Y, Hua F, Shao L, Li J, Chen Y, Yu Y, Shen Z. The enhanced effect and underlying mechanisms of mesenchymal stem cells with IL-33 overexpression on myocardial infarction. Stem Cell Res Ther. 2019 Sep 23;10(1):295. doi: 10.1186/s13287-019-1392-9. PMID: 31547872; PMCID: PMC6757387.
37. Mader EK, Butler G, Dowdy SC, Mariani A, Knutson KL, Federspiel MJ, Russell SJ, Galanis E, Dietz AB, Peng KW. Optimizing patient derived mesenchymal stem cells as virus carriers for a phase I clinical trial in ovarian cancer. J Transl Med. 2013 Jan 24;11:20. doi: 10.1186/1479-5876-11-20. PMID: 23347343; PMCID: PMC3567956.

Tables

Table 1: Description of clinical-grade MSCs

ID	*Source*	*Condition*
211	Fat biopsy	Healthy
258	Fat biopsy	Healthy
540	Fat biopsy	Amyotrophic lateral sclerosis
536	Fat biopsy	Ovarian Cancer
569	Fat biopsy	Amyotrophic lateral sclerosis
528	Fat biopsy	ARAS
544	Fat biopsy	ARAS
553	Fat biopsy	ARAS
554	Fat biopsy	ARAS
565	Fat biopsy	ARAS
535	Fat biopsy	Crohns Disease
566	Fat biopsy	Ovarian cancer
965	Fat biopsy	MSA
538	Fat biopsy	MSA
537	Fat biopsy	MSA
559	Fat biopsy	MSA
750-1	Bone marrow	Healthy
750-3	Bone marrow	Healthy
Abbreviations: ARAS – artherosclerotic renal artery stenosis, MSA – multiple system atrophy		

Table 2: Top 10 categories from David 6.8 analysis of differentially expressed genes in CD36+ enriched and depleted AMSCs

CD36+ Enriched			*CD36+ Depleted*		
Enrichment Score	Functional Categories	Database	Enrichment Score	Functional Categories	Database
3.49	Glycoprotein	UP_KEYWORDS	13.24	Glycoprotein	UP_KEYWORDS
3.17	Membrane	UP_KEYWORDS	13.01	Secreted	UP_KEYWORDS
2.09	cell adhesion	GOTERM_BP_DIRECT	3.9	IGFBP, N-terminal	INTERPRO
2.07	Collagen	UP_KEYWORDS	3.24	Protease	UP_KEYWORDS
2.05	ECM-receptor interaction	KEGG_PATHWAY	2.67	Fibronectin, type III	INTERPRO
1.69	extracellular space	GOTERM_CC_DIRECT	2.09	Membrane	UP_KEYWORDS
1.56	Cadherin	INTERPRO	1.71	Thrombospondin, type 1 repeat	INTERPRO
1.28	Muscle protein	UP_KEYWORDS	1.68	Focal adhesion	KEGG_PATHWAY
1.1	EGF	SMART	1.61	Collagen	UP_KEYWORDS
0.98	Calcium transport	UP_KEYWORDS	1.1	Lipid metabolism	UP_KEYWORDS

Figures

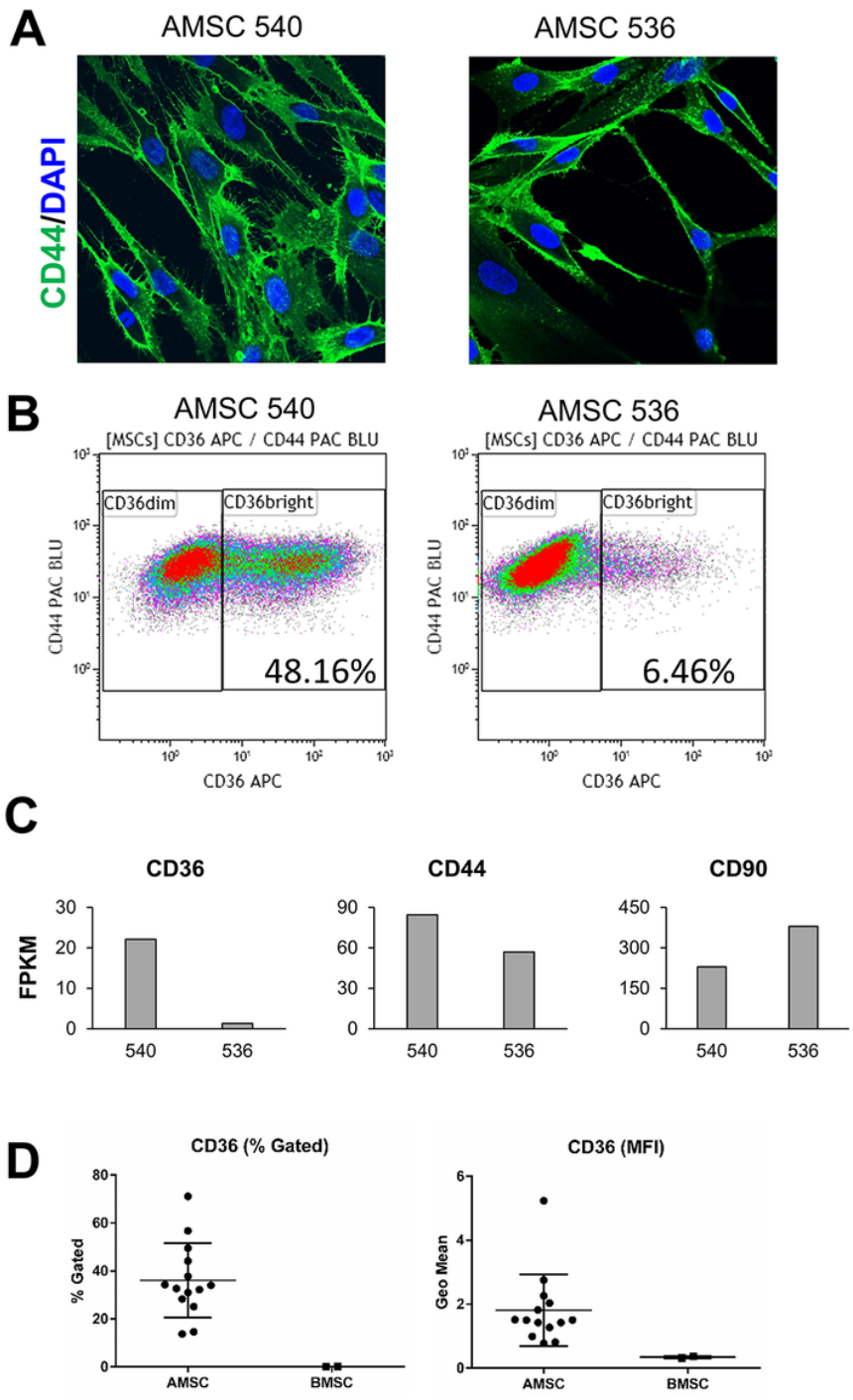

Figure 1

CD36 staining on clinical-grade adipose-derived mesenchymal stromal cells (AMSCs) show biphasic expression. A. Immunofluorescent staining of CD44 for two AMSCs donors show the expression of the classical surface marker. B. Representative flow cytometry scatter plots of CD36+ and CD44+ stained AMSCs from two donors show two cell populations with dim and bright CD36+ expression. CD36+ bright population have variable populations frequencies between the two donors. C. Transcript abundance from RNA-sequencing data of the two MSC donors shows validates the higher expression of CD36 in 540 compared 536, whereas CD44 and CD90 are similar between the donors. D. Cell surface expression of CD36 was also unique to AMSCs and not expressed on clinical-grade BMSCs grown in human platelet lysate.

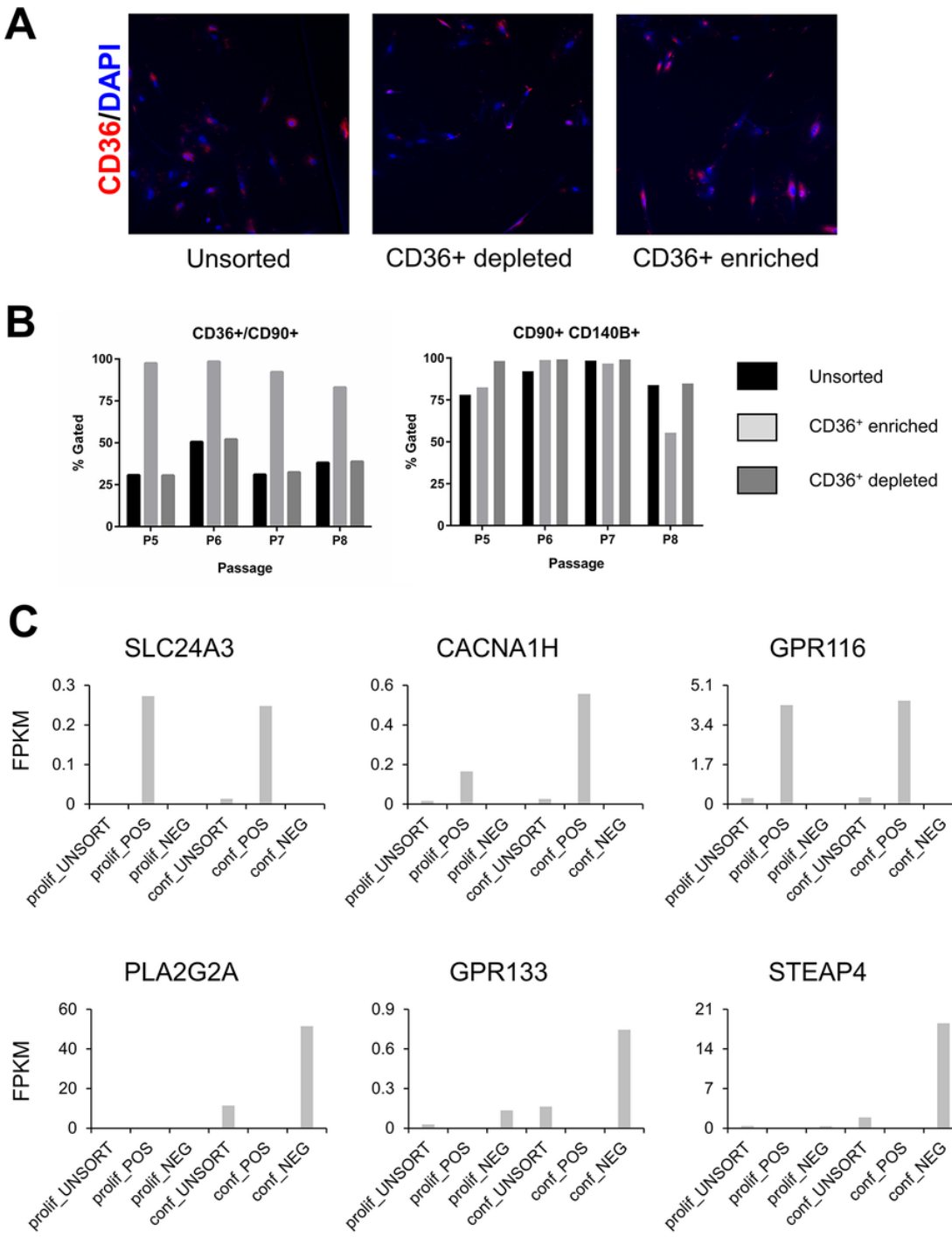

Figure 2

Identification of a CD36+ enriched AMSCs stable subpopulation with enhanced expression of calcium transporting genes. Enrichment or depletion of CD36+ AMSCs were obtained by magnetic cell sorting. A. Immunofluorescent staining of CD36 shows enhanced expression on enriched cells compared to depleted or unsorted cells. B. Serial passaging and flow cytometry analysis for CD36 and CD90 shows maintenance of CD36+ positivity over three passages in enriched cells (left), whereas CD90+/CD140B+ expression is similar between the groups over the three passages (right). RNA-sequencing analysis of proliferating and confluent unsorted, CD36+ enriched, and CD36+ depleted AMSCs were found to have enhanced expression of calcium

transport genes including SCL24A3, CACNA1H, and GPR116. Whereas genes associated with adipocytes (STEAP3) and fat metabolism (PLA2G2A) were more abundant in unsorted and CD36+ depleted AMSCs.

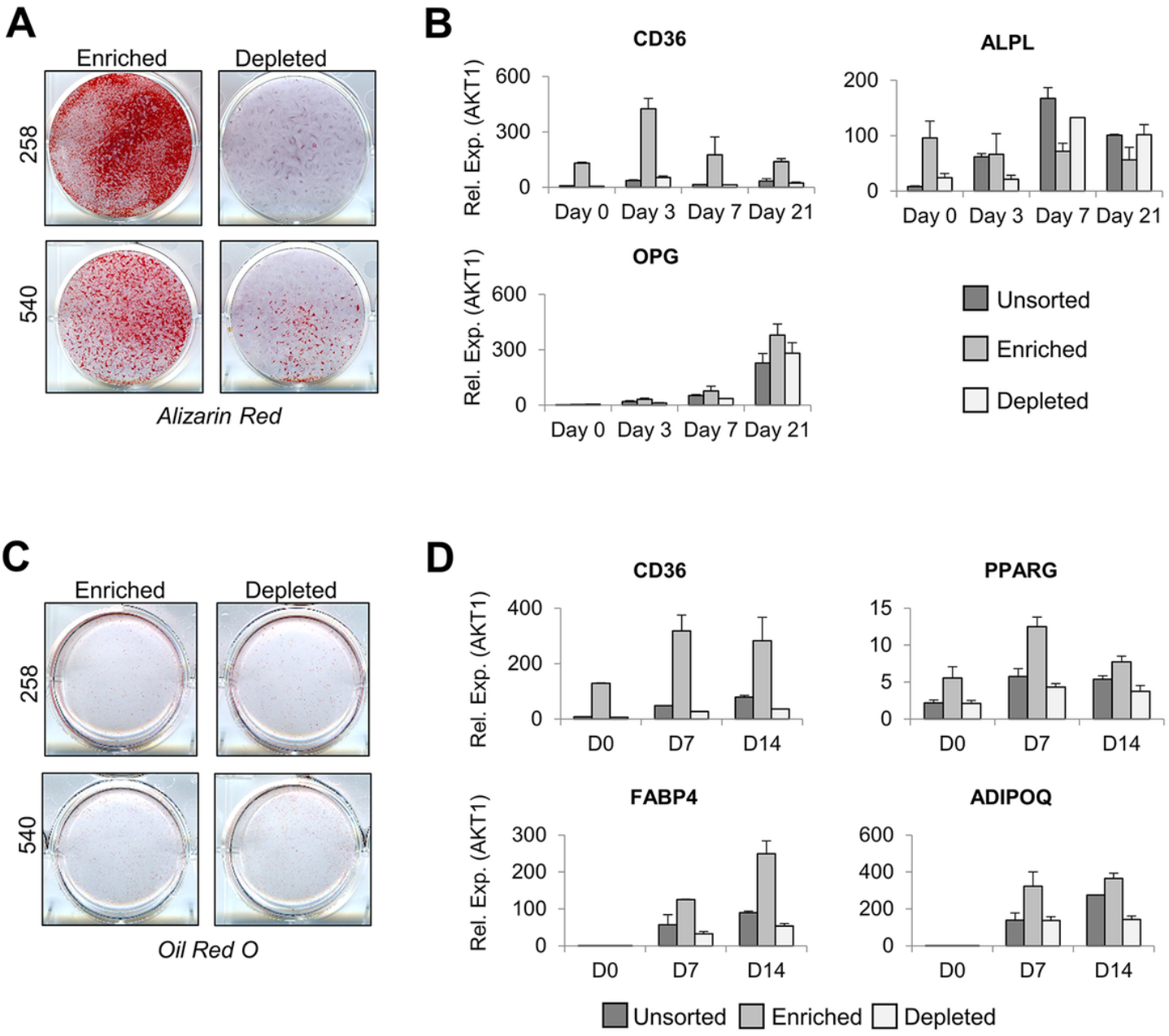

Figure 3

CD36+ enriched AMSCs show enhanced osteogenic potential. A. Osteogenic differentiation of unsorted, CD36+ enriched and depleted AMSCs for up to 21 days showed enhanced calcium deposition as indicated by Alizarin Red staining. B. Relative expression of osteogenic markers show upregulation of alkaline phosphatase (ALPL) at day 0. Osteoprotegrin (OPG or TNFRSF11B) was also more abundant from day 3-21. Adipogenic differentiation was also evaluated in AMSC subpopulations and lipid droplet staining with Oil Red O at day 14 was not different

between CD36+ enriched and depleted AMSCs (C). However, relative expression of adipogenic markers was enhanced in CD36+ enriched AMSCs compared to unsorted and CD36+ depleted cells (D).

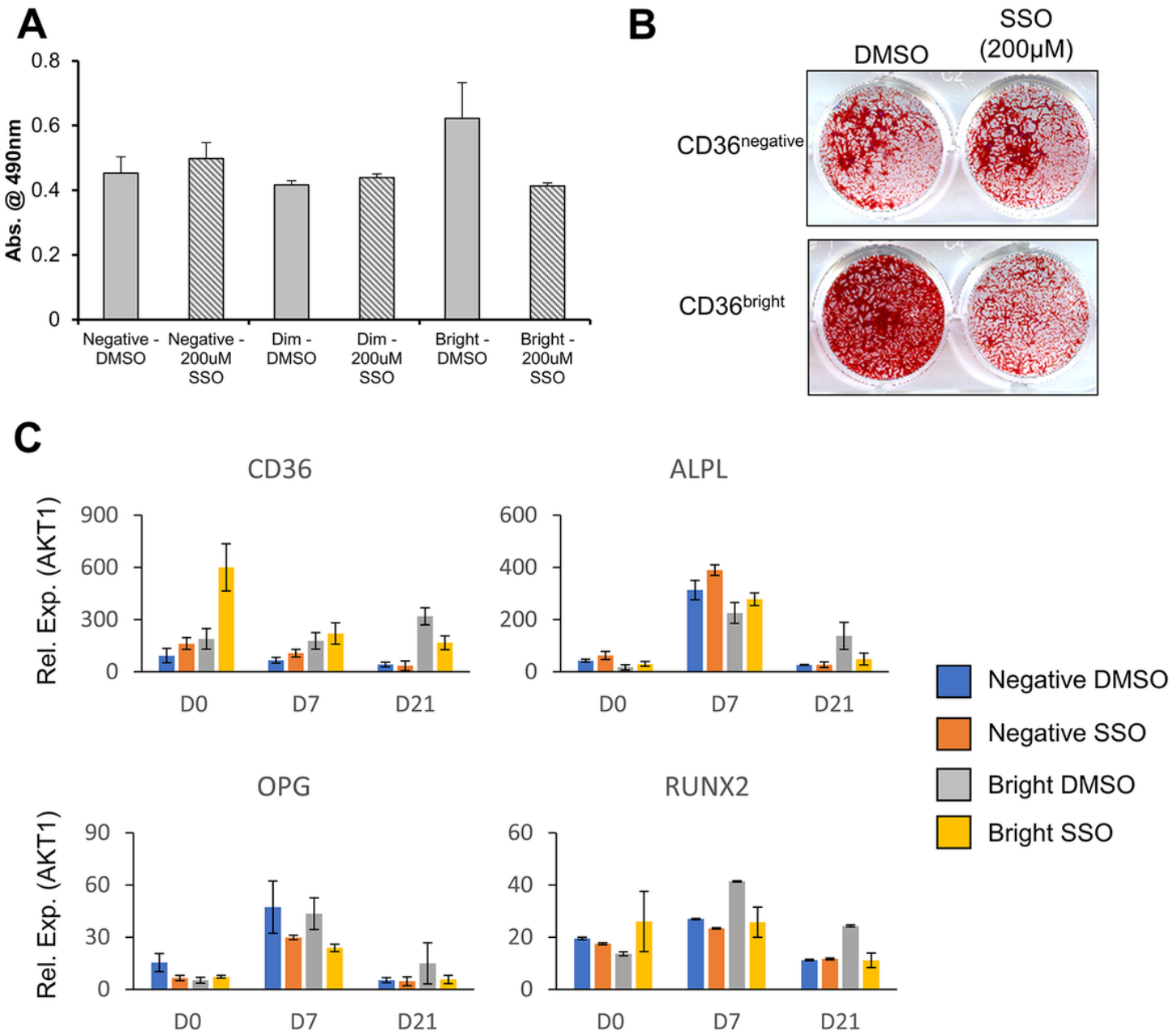

Figure 4

Pro-osteogenic potential of CD36+ enriched AMSCs directly mediated by CD36 function. AMSCs were sorted by CD36 expression using flow cytometry to isolate a negative, CD36+ dim and CD36+ bright subpopulations. A. Sorted AMSCs were treated with the CD36 inhibitor Sulfosuccinimidyl Oleate (SSO) or vehicle control (DMSO) and metabolic activity was measured using the MTS assay. DMSO treated CD36+ bright exhibited higher metabolic activity compared to CD36+ negative AMSCs. Treatment with 200μM of SSO reduced the metabolic activity to similar levels as CD36+ negative and dim AMSCs. CD36+ bright and negative AMSCs were treated

with DMSO or 200μM of SSO for three days and then osteogenic differentiation was induced using osteogenic cocktail. B. Alizarin Red staining at day 14 revealed reduced calcium deposition in CD36+ bright AMSCs treated with SSO, whereas staining of CD36+ negative AMSC was unaffected. C. Relative expression of ALPL and RUNX2 were reduced in CD36+ bright AMSCs treated with SSO at day 21. OPG was downregulated in both CD36+ positive and negative AMSCs on days 7 and 21.

Supplementary Files

This is a list of supplementary files associated with this preprint. Click to download.

- SupplementalFigure1.tif
- SupplementalFigure2.tif
- SupplementalTable1.xlsx
- SupplementalTable2.xlsx
- SupplementalTable3.xlsx
- SupplementalTable4.xlsx